communications earth & environment

ARTICLE

https://doi.org/10.1038/s43247-022-00383-z OPEN

Rapid remote monitoring reveals spatial and temporal hotspots of carbon loss in Africa's rainforests

Ovidiu Csillik[1✉], Johannes Reiche[1], Veronique De Sy[1], Arnan Araza[1] & Martin Herold[1,2]

Spatially explicit monitoring of tropical forest aboveground carbon is an important prerequisite for better targeting and assessing forest conservation efforts and more transparent reporting of carbon losses. Here, we combine near-real-time forest disturbance alerts based on all-weather radar data with aboveground carbon stocks to provide carbon loss estimates at high spatial and temporal resolution for the rainforests of Africa. We identified spatial and temporal hotspots of carbon loss for 2019 and 2020 for the 23 countries analyzed, led by different drivers of forest disturbance. We found that 75.7% of total annual carbon loss in the Central African Republic happened within the first three months of 2020, while 89% of the annual carbon loss in Madagascar occurred within the last five months of 2020. Our detailed spatiotemporal mapping of carbon loss creates opportunities for much more transparent, timely, and efficient assessments of forest carbon changes both at the level of specific activities, for national-level GHG reporting, and large area comparative analysis.

[1] Laboratory of Geo-Information Science and Remote Sensing, Wageningen University and Research, Wageningen, The Netherlands. [2] Helmholtz GFZ German Research Centre for Geosciences, Section 1.4 Remote Sensing and Geoinformatics, Potsdam, Germany. ✉email: ovidiu.csillik@gmail.com

Conserving and reducing the loss of rainforests is among the most effective solutions for mitigating climate change and for preserving key ecosystem services[1]. International and national initiatives related to the Paris Climate Agreement stimulate and implement targeted activities for avoiding tropical forest loss[2]. Their success, however, depends on suitable information on where and why forests are changing to define suitable policies and actions, to support implementation and enforcement on the ground, and to provide robust reporting on the progress and performance of such activities[3,4]. Forest carbon monitoring efforts have evolved, but limited spatial detail and timeliness hinder their usefulness for tracking collective progress towards forest-specific climate mitigation goals. This is a particular issue for Africa's humid forest changes that remain poorly understood and quantified[5,6]. The fact that the most recent national forest inventories (NFIs) of countries in this region are 4.5 ± 3.2 years old (Supplementary Table 1) highlights that available data are not serving the action-oriented nature of ongoing forest-related mitigation schemes.

Rapid detection of forest disturbances in Africa has already proven to decrease the probability of deforestation by 18%, with an estimated social cost of carbon for avoided deforestation between US$149 million and US$696 million[7]. Two main causes of forest disturbance in the Congo basin between 2000 and 2014 were small-scale clearing for agriculture (84%) and selective logging (10%), with regional differences[8]. For example, more than 60% of forest disturbances in Gabon are due to selective logging and more than 90% of disturbances in the Democratic Republic of the Congo (DRC) and the Central African Republic are due to small-scale agriculture[8]. West and East African tropical forests, including Madagascar, have lost almost all the forest extent in the last decades[9], while the last two largest tropical forest fragments in Africa, both located in the DRC are at immediate threat due to continuing expansion of rural populations into remote forests[10]. A long-term future prediction indicates a decline in the African tropical forest carbon sink[11].

Monitoring forest carbon changes using remote sensing technologies has become increasingly feasible[12–14] driven by the abundance of multi-source satellite time-series data for tracking forest changes[15,16] and forest biomass and carbon stocks[14,17]. Driven by the open access availability of Sentinel-1 data, radar-based approaches are now operationally available to overcome cloud-cover issues in large area tropical forest monitoring and assess small-scale disturbances in a matter of days at 10 m spatial scale[18]. Such information can be used to track changes at spatiotemporal scales at which human activities affecting forests and land use are operating. This creates opportunities for much more transparent, timely, and efficient assessments of forest carbon changes both at the level of specific activities, for national-level GHG reporting, and large area comparative analysis.

Here, we present a high-resolution spatially explicit rapid monitoring of local carbon loss in Africa's humid tropical forest by combining data of radar-based forest change alerts and spatial carbon stock estimates. We define local carbon loss as the complete or partial potential loss of carbon that can later be emitted into the atmosphere. We analyzed the spatiotemporal dynamics of carbon loss in 2019 and 2020 by combining aboveground carbon estimates, derived from a combination of best available remote sensing and field data, with near-real-time radar-based forest disturbance alerts, at a spatial scale of 10 m with monthly intervals. We separate between high and low confidence alerts and provide uncertainty estimates at the pixel and country-level by combining the uncertainties of the carbon map with commission and omission errors of the alerts. We analyzed 23 countries with a wide variety of spatiotemporal patterns of carbon loss and found correlations between the two years analyzed reaching up to 0.94.

Results and discussion

Continental, regional, and local spatiotemporal patterns of carbon loss. For Africa's primary tropical humid forest, carbon losses due to forest disturbances reached 42.2 ± 5.1 MtC yr^{-1} (mean ± standard deviation, where MtC yr^{-1} is one million metric tons of carbon loss per year) in 2019 and 53.4 ± 6.5 MtC yr^{-1} in 2020. Just 9 countries out of the 23 analyzed accounted for 95.0% of total gross losses in 2019 and 94.3% in 2020. These countries contain about 95.7% of all primary tropical humid forests of Africa, with the DRC accounting for 52.8%, Gabon 11.8%, the Republic of the Congo 11.0%, and Cameroon 9.8%. Of these, DRC and Cameroon were responsible for 49.3% and 19.1% of losses in 2019 and 44.7% and 20.6% in 2020. DRC and Cameroon had an annual increase of 15.0% and 36.5% respectively, between 2019 and 2020. From countries with at least 1 MtC emitted in the two years analyzed, Madagascar had the highest annual increase in carbon loss (+153.9%), while Equatorial Guinea is the only country with a decrease in carbon loss (−20.1%). Extending the carbon loss analysis for both past and future will help to better understand these variations and whether the COVID-19 global pandemic had any influence on the general increase between 2019 and 2020[19]. While the absolute numbers for carbon loss estimates should be treated carefully and a sample-based approach should be preferred for an unbiased estimate of absolute numbers[20], we focused our analysis on the trends of carbon loss at the continental, country, and local scale (Fig. 1 and Supplementary Fig. 1).

The high temporal detail of the analysis revealed various monthly patterns of carbon losses for countries, highly related to local rainfall patterns[18] (Fig. 2). Countries like Cameroon, Liberia, Nigeria, Central African Republic (CAR), and Madagascar showed a clear dry-wet seasonal variation in carbon loss per year, while the Republic of the Congo and the DRC, due to their latitudinal extent, exhibited two dry-wet season variations per year with varying intensities (Fig. 2). The seasonal variation can be explained by higher accessibility to forests during the dry months when activities related to smallholder agriculture and logging are more feasible than in the wet season when many roads become inaccessible.

One of the highest differences between the months with the most and the least carbon losses was found for Madagascar (72 times more carbon loss in March compared to November 2019). In CAR, the three consecutive months with the highest cumulative carbon loss (January to March 2020) contributed to 75.7% of the total annual loss (between February and April 2020), in Nigeria 73.9% (January to March 2020), Liberia 73.1% (February to April 2020), Madagascar 70.7% (September to November 2020), and Cameroon 62.2% (January to March 2020). Lower percentages were found for countries with mixed seasonality and patterns, like DRC 36.7% (January to March 2020), and the Republic of the Congo 32.8% (January to March 2020) (Fig. 2). For the latter two countries, we expect better-defined peaks of carbon loss at local scales, where climatic conditions are not mixed. The annual cumulative carbon loss (%) per country (Fig. 3) showed that Liberia, Nigeria, CAR, and Cameroon reached between 70-90% of their annual carbon loss in April, while Madagascar reached 60% in October. The DRC, Gabon, Republic of the Congo, Equatorial Guinea, and Ghana have a more gradual monthly increase of cumulative carbon loss with less contrasting seasonality effects. Monthly patterns of carbon losses between the two years analyzed resulted in a correlation coefficient of 0.94 for the CAR, 0.92 for the DRC, 0.91 for Madagascar, 0.90 for Gabon, and 0.83 for Cameroon (Supplementary Fig. 2). For the Republic of the Congo, the two years correlated 0.51. Knowing the peak months of carbon loss

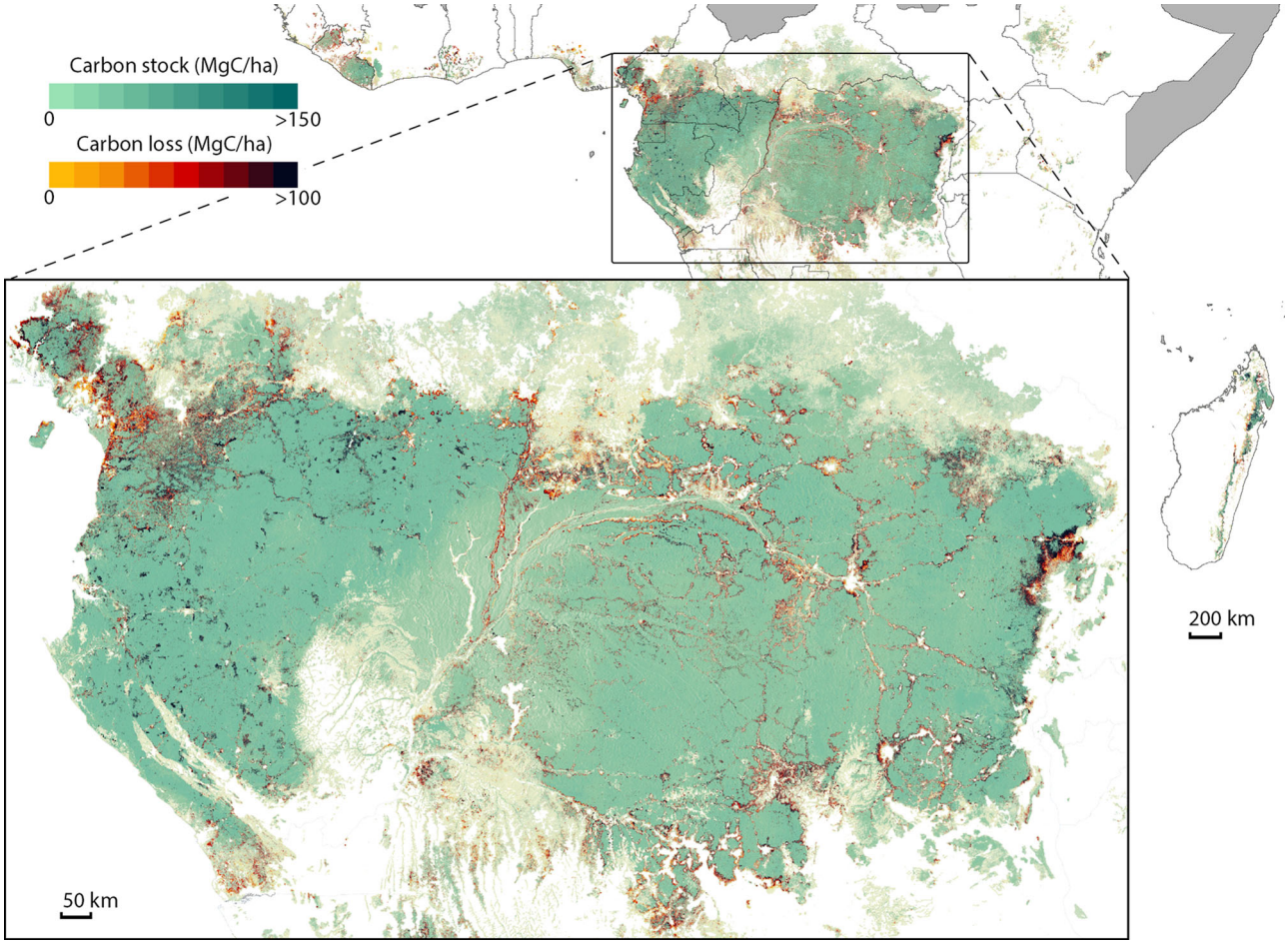

Fig. 1 Carbon loss across Africa's rainforests. We analyzed 23 countries containing primary moist forest. The aboveground carbon stock (green palette) underlies the carbon loss estimations (red palette). Several hotspots can be seen across these regions. The uncertainties of the carbon loss estimations are expressed as standard deviations and shown in Supplementary Fig. 1.

for each country and that these patterns are repeatable from one year to another can contribute to better target and prioritize enforcement activities, as well as predicting future patterns and early reporting of annual forest carbon losses.

Several hotspots of carbon losses can be seen in Fig. 1. The high spatial and temporal details of our analysis are shown in Fig. 4, where several local examples with different drivers of forest disturbances are shown, like logging roads, selective logging, mining, oil palm plantations, urban expansion, and small-holder agriculture. This kind of information, coupled with auxiliary datasets (e.g., legal concessions, protected areas) can identify the legality of forest disturbance[21].

Implications of rapid monitoring of local carbon loss. Near-real time alerts combined with biomass maps result in spatially explicit forest carbon loss, unlike global tabular statistics of national data[22,23]. We provide new insights into the spatio-temporal dynamics of carbon loss with consistent assessment of accuracy that could enable transparency and completeness for countries reporting on their REDD + progress to the UNFCCC[24]. We provide monthly carbon loss estimates that could play a key role in local, national, and international forest initiatives for global carbon policy goals[25]. Such a system can be implemented with minimal costs and is based on open-source datasets and Google Earth Engine cloud computing platform[26], thus enabling cost-effective national monitoring of forest carbon loss[7]. Providing rapid reporting on the location, time, and amount of carbon lost across Africa's primary humid forest will help undertake immediate action to protect and conserve carbon-rich threatened forests. Furthermore, countries will be able to predict and estimate their annual carbon loss before a reporting period ends, thus having the opportunity to adjust their practices to meet their country-specific commitments for climate change mitigation initiatives.

Limitations and future improvements. We used the RADD alerts (Radar for Detecting Deforestation)[18] with a minimum mapping unit (MMU) of 0.2 ha as accuracy estimates were available for this MMU. Events smaller than 0.2 ha would add to the total carbon loss but are by nature associated with higher uncertainties[18]. The implications of the RADD alerts using a global humid tropical forest product as a forest baseline for 2018[16,27,28] are twofold. First, the global nature of this product might result in inconsistencies at the local level[18]. Second, because the forest cover loss information used to generate the forest baseline is based on optical Landsat data, persistent cloud cover in the second half of 2018 in some areas led to missed reporting of forest disturbances, thus being detected at the beginning of 2019 by the RADD alerts. This possible overestimation of carbon loss at the start of 2019 is not an issue for a near-real-time alerting system since later months are not affected. Furthermore, the alerts do not distinguish between human-induced disturbances and natural forest disturbances[18]. When a new forest disturbance alert is detected, it will be confirmed or

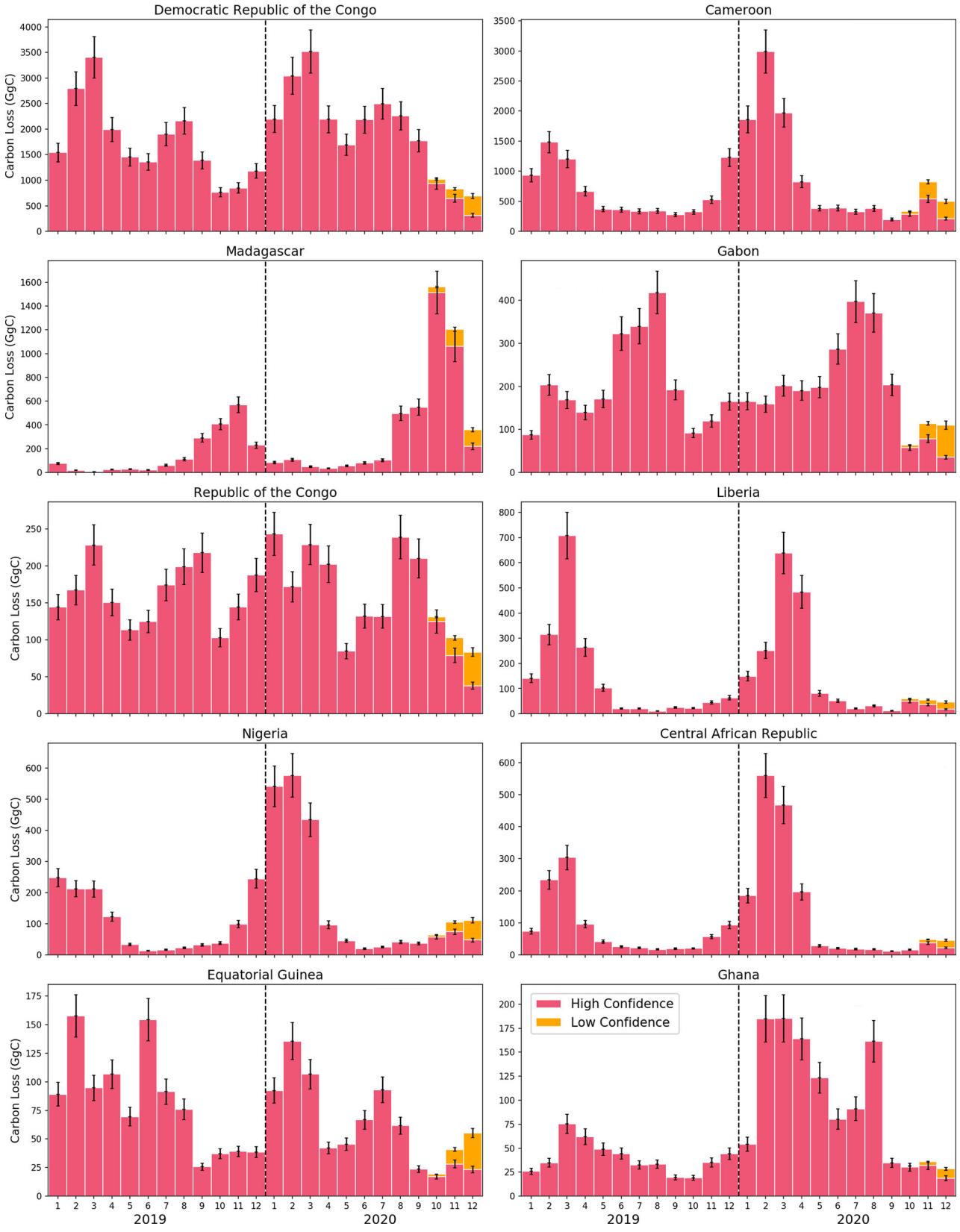

Fig. 2 Temporal patterns of carbon loss for the top 10 countries. We show monthly statistics for 2019 and 2020 and the associated uncertainty (black lines). We separate between high (red bars) and low (yellow bars) confidence alerts, the latter showing up for the last 3 months of 2020.

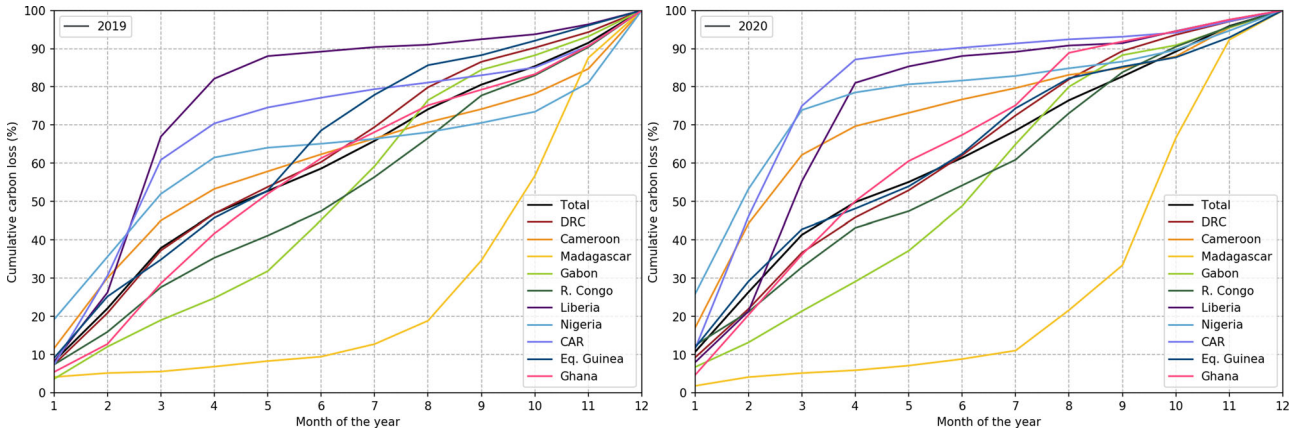

Fig. 3 Annual cumulative carbon loss (%) for both years analyzed, 2019 and 2020. Africa's total cumulative carbon loss is shown with a black line. The 10 topmost emitting countries out of 23 countries analyzed are shown and represented by distinct colored lines.

rejected within 90 days by subsequent Sentinel-1 images[18]. That is why our carbon loss reporting separates between high and low confidence alerts for the last three months of 2020, which is common for most forest disturbance alerting products[18,29]. We separated all the alerts into core and boundary pixels. Core alerts represent complete tree cover removal and we assumed complete carbon loss within a pixel. For boundary alerts, we assumed a 50% carbon loss since these mainly represent forest disturbances with partial tree cover removal. Detecting and quantifying the level of degradation remains challenging and future developments will minimize this uncertainty by providing variable percentages of degraded forest[30]. The timeliness and spatial details of future forest disturbance alerting products will improve with the availability of open access long-wavelength radar data from near-future satellite missions (e.g., NISAR L-band SAR in 2023[31]), by using a combination of optical and radar forest disturbance alert products, and integration with high-resolution satellite products.

We relied on an aboveground biomass baseline map from 2018[32], prior to RADD alerts starting from 2019. Biomass estimation for the tropical moist forests is based on ALOS-2 PALSAR-2 L-band satellite and its usage needs to account for the local biases, especially underestimating AGB values higher than 250 Mg ha^{-1} (ref. [32]). Although we reduced this underestimation by adjusting the AGB map based on ground field data, more research is needed on providing up-to-date high-resolution aboveground carbon estimates[33] that could further increase the accuracy of local carbon loss estimation. Radar-based estimation of forest carbon stocks is challenging over mountainous terrain and is less accurate in complex canopies[3] and future integration of radar and optical satellite data will provide more robust estimates[33]. Nevertheless, new spaceborne missions (e.g., GEDI[34], BIOMASS[35]) will provide an unprecedented amount of forest structure samples that will improve the algorithms and thus the final accuracy of aboveground biomass estimates.

We focused on exploring and analyzing local carbon losses and showing high temporal and spatial patterns of carbon losses. We showed the country statistics to emphasize the temporal dynamics of carbon losses and compare the temporal profiles across our study region. Our approach was not to provide stratified area estimations[36] associated with forest disturbances but we used this concept in the sense that we had a stratified sample of higher quality reference data[18] to estimate the omission and commission errors and consider those in our uncertainty estimation on the pixel level. The analysis showed that omission and commission errors are small and rather balanced, and thus do not result in a major area bias for the forest disturbances. The uncertainties of the aboveground biomass product[32] were adjusted for known regional biases using regional forest biomass plot data sources. With this approach, the original aboveground biomass map bias was partly corrected using a model-based approach deemed to be an alternative to a sample-based approach whenever country data are unavailable[37]. Our uncertainty analysis and error reduction showed that we expect only minor bias in the forest disturbance and the biomass data and the remaining uncertainties are propagated in our pixel-based uncertainty layer.

Conclusions

We introduce an analysis framework to estimate tropical forest aboveground carbon loss with high-spatial and temporal resolution that provides suitable information to enhance implementation and enforcement on the ground. This type of spatially explicit analysis will benefit all actors involved in climate change mitigation policies and actions, with improved transparency, transferability, and speed of reporting carbon losses promptly. Our framework provides a continentally comprehensive dataset on carbon losses that can be easily adapted to ingest new datasets, thus providing a benchmarking approach that will enhance the capacity of countries to track the progress towards the goals of the Paris Agreement at multiple scales.

Methods

Study area. The study area is represented by the primary tropical humid forest of Africa and covers 23 countries. The primary tropical forest is defined as mature natural tropical forest cover that has not been completely cleared and regrown in recent history[27]. We created a reference primary tropical humid forest mask for 2018 using the extent of these forests in 2001[27], from which we excluded the forest loss between 2001 and 2018[16] and mangroves[28].

Forest disturbance alerts. We used the RADD alerts (Radar for Detecting Deforestation) based on Sentinel-1 data for the years 2019 and 2020[18]. Forest disturbance is defined as the complete or partial removal of tree cover within a 10×10 m pixel (0.01 ha)[18]. Complete removal of tree cover is associated with a stand-replacement disturbance at the pixel scale, while partial removal mainly represents disturbances associated with boundary pixels and selective logging[18]. The alerts are based on Sentinel-1 radar satellite time-series data and a forest disturbance alert is triggered and confirmed with high confidence after multiple consecutive observations using Bayesian updating[18]. There are two types of alerts: (1) low confidence alerts are provided for a forest disturbance probability >0.85 and (2) high confidence alerts for forest disturbance probabilities >0.975, within a maximum period of 90 days from first detection[18]. Due to this timeframe of confirming alerts, analyzing 2019 and 2020 alerts will result in the last three months of 2020 having both high and low confidence alerts. We used an MMU of 0.2 ha since at this MMU the alerts were validated[18]. The user's and producer's accuracies of high confidence alerts of forest disturbance larger than or equal to 0.2 ha were 97.6% and 95.0%, respectively, using stratified random sampling and a buffer zone around alerts to ensure a good estimate of the omission error[36]. For each alert pixel, we computed the number of neighboring alert pixels in an eight

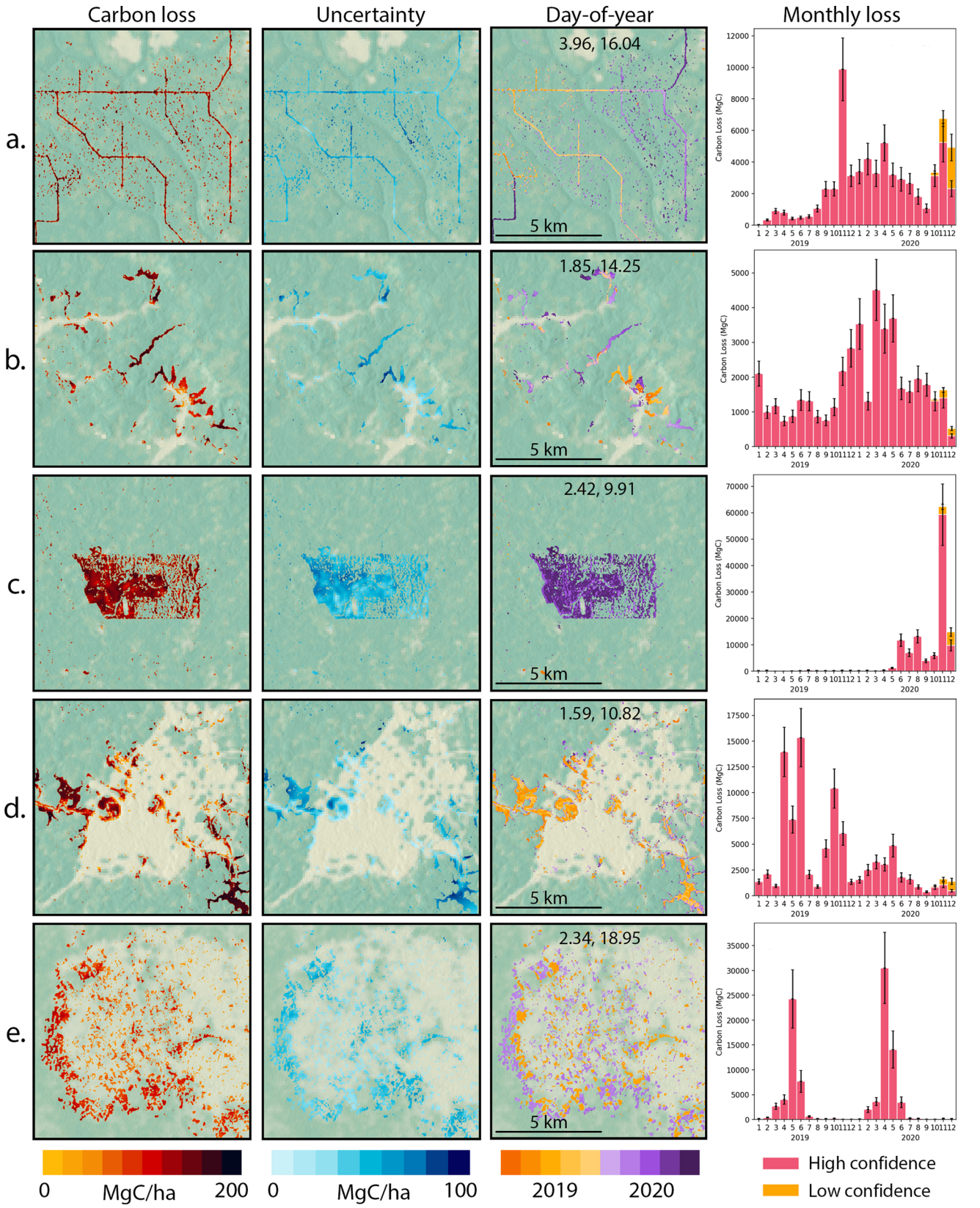

Fig. 4 Local examples of approx. 10 × 10 km in extent showing different spatiotemporal patterns and drivers of carbon loss. The first column shows the carbon loss, the second column the associated uncertainty, the third column the day-of-the-year when the loss occurred, and the last column shows the monthly distribution of carbon loss and associated uncertainty for each local example. The center coordinates of each location are shown in the third column as latitude and longitude. Exact locations are shown in Supplementary Fig. 3. **a** Logging roads and selective logging in the Central African Republic, **b** mining of gold and titanium in the Republic of the Congo, **c** development of an oil palm plantation in Cameroon, **d** forest disturbance related to building a new capital city in Equatorial Guinea, and **e** small-scale agriculture expansion at the edge of the forest in the DRC.

connected direction and separated between core alerts (pixels fully surrounded by 8 alert pixels) and boundary alerts (pixels with less than 8 neighboring alert pixels)[18].

Aboveground biomass estimation. We used the single-date spatially explicit ESA Climate Change Initiative (CCI) Version 2 aboveground biomass map for 2018 with per-pixel associated accuracy (standard deviation) at a spatial resolution of 100 m[32]. The map was obtained based on Sentinel-1 C-band and ALOS-2 PALSAR-2 L-band data using an algorithm that inverts a semi-empirical model relating the forest backscatter to canopy density and height and then transformed to AGB using allometric equations[32]. The per-pixel standard deviation is calculated by propagating individual uncertainties of the SAR measurement and the modeling framework[32]. The AGB estimates for the wet tropics depend solely on the L-band backscatter data that is prone to local biases related to wet conditions and limited sensitivity to biomass in moderate to high biomass forests[32]. This resulted in a non-uniform bias or the overestimation of low biomass and underestimation of high biomass (>250 MgC/ha), the latter being driven by signal saturation of remote sensing images[38]. This map bias can be modeled since different forest types, climatic gradients, topography, and aboveground biomass itself have been found to affect bias in biomass predictions[39,40]. Map bias can be modeled only after accounting for the sources of uncertainties from the map and the plot data used for validation[41].

A collection of research and forestry plots was compared with the CCI Biomass map for 2018 to derive the map bias[41]. Then, bias was modeled as a function of the AGB map and its textural properties as well as other spatially exhaustive covariates such as biome[42], topographic variables (aspect and slope), forest fractional cover[43], and the standard deviation layer of the AGB map using a random forest model[44]. The bias model followed a 10-fold cross-validation and was assessed through Root Mean Square Error (RMSE) (42.24 Mg/ha) and Mean Absolute Error (MAE) (29.25 Mg/ha). The predictive power of the covariates was also evaluated using variable importance measures while the sensitivity of the modeled trends to its inputs was assessed using partial dependence plots[45]. Statistical significance of predicted bias was assessed using the prediction standard errors obtained with the infinitesimal jack-knife approach[46]. Only those statistically significant bias pixels were used to correct AGB map pixels. We ultimately converted the bias-adjusted AGB and associated standard deviation to carbon values using a conversion factor of 0.47[47].

Aboveground carbon loss and uncertainties. We combined the forest disturbance alerts and aboveground carbon stocks to estimate local carbon loss at two different spatial scales, 10 m (0.01 ha) and 100 m (1 ha). The two spatial scales matched those of the two main datasets used, the alerts and biomass estimates, and thus easier integration with either of them can be achieved. Carbon loss at 10 m was calculated as the percentage of the 0.01 ha of the alert pixel within the 1 ha area of an aboveground carbon pixel (1%). Losses at 1 ha were computed as the percentage of disturbance alerts within a 1 ha pixel from the total aboveground carbon stored by that 1 ha pixel. For both approaches, a distinction between high and low confidence and core and boundary disturbance alerts was made. We considered complete removal of tree cover and, therefore, complete carbon loss (100%) for core alerts and partial carbon loss (50%) for boundary alerts.

We estimated the uncertainty of carbon loss estimates per pixel and at the country level based on the propagation of the AGB standard deviation and the commission and omission errors of the alerts.

We defined a model of carbon loss (CL) (Eq. 1):

$$\mathrm{CL} = \mathrm{AGC} \times i \tag{1}$$

where AGC represents the aboveground carbon in forest biomass in a certain pixel and i is an indicator that is 1 if a pixel is labeled as disturbed and 0 otherwise. For the case a pixel is labeled as being disturbed, we combined the variance of AGC and the commission error of the alerts (2.4%). The probability of a pixel labeled as disturbed ($i = 1$) to actually be disturbed is 0.976 and the variance of this binomial trial is 0.0234. We further used the formula for the variance of a product of two uncorrelated random variables, resulting in the variance of carbon loss estimate (var(CL)) to be computed as (Eq. 2):

$$\mathrm{var(CL)} = \mathrm{AGC}^2 \times 0.0234 + 0.976^2 \times \mathrm{stdev_{AGC}}^2 + 0.0234 \times \mathrm{stdev_{AGC}}^2 \tag{2}$$

For the case a pixel was not labeled as being disturbed, thus considered intact forest ($i = 0$), it has an expected disturbance probability of 0.05 due to the omission error of the alerts. Its variance would then be 0.0475 and applying the corresponding formula from above would result in the variance of the carbon loss for an undisturbed pixel to be (Eq. 3):

$$\mathrm{var(CL)} = \mathrm{AGC}^2 \times 0.0475 + 0.05^2 \times \mathrm{stdev_{AGC}}^2 + 0.0475 \times \mathrm{stdev_{AGC}}^2 \tag{3}$$

We assumed complete dependence of the uncertainties when we scaled up to the country level, which resulted in a conservative approach since data dependence always results in larger uncertainty values[48]. As a first step, we calculated the standard deviation at the aggregated country scale as the sum of standard deviations at the pixel level[48]. In computing carbon loss uncertainties, we did not consider land cover successions or the main drivers of carbon loss. We then expanded the formula above to calculate the variance of a product of multiple uncorrelated random variables (AGC, commission, omission errors, and their variances) and computed the country-scale variance of carbon loss ($\mathrm{var(CL)_{country}}$) as (Eq. 4):

$$\begin{aligned}\mathrm{var(CL)_{country}} = {} & \left(\mathrm{stdev(AGC)}^2 + \mathrm{AGC}^2\right) \times \left(0.0234 + 0.976^2\right) \\ & \times \left(0.0475 + 0.05^2\right) - \mathrm{AGC}^2 \times 0.976^2 \times 0.05^2\end{aligned} \tag{4}$$

Ultimately, we calculated the square root of the resulted variances and expressed the per-pixel and country-scale carbon loss statistics and uncertainties as mean ± standard deviation.

Data availability

The data used for this study are available from the ESA Climate Change Initiative Biomass (https://climate.esa.int/en/projects/biomass/) and RADD alerts (http://radd-alert.wur.nl/). The data resulted from our study are available as Google Earth Engine assets at https://code.earthengine.google.com/?asset=users/cskovidiu/AfricaCarbonLoss (carbon loss and date of loss) and https://code.earthengine.google.com/?asset=users/cskovidiu/AfricaCarbonLoss_SD (standard deviation of carbon loss).

Code availability

The code is available upon request from the corresponding author.

Received: 3 September 2021; Accepted: 28 January 2022;
Published online: 04 March 2022

References

1. Bastin, J.-F. et al. The global tree restoration potential. *Science* **365**, 76–79 (2019).
2. Bos, A. B. et al. Global data and tools for local forest cover loss and REDD+ performance assessment: Accuracy, uncertainty, complementarity and impact. *Int. J. Appl. Earth Obs. Geoinf.* **80**, 295–311 (2019).
3. Gibbs, H. K., Brown, S., Niles, J. O. & Foley, J. A. Monitoring and estimating tropical forest carbon stocks: making REDD a reality. *Environ. Res. Lett.* **2**, 045023 (2007).
4. Nesha, M. K. et al. An assessment of data sources, data quality and changes in national forest monitoring capacities in the Global Forest Resources Assessment 2005–2020. *Environ. Res. Lett.* **16**, 054029 (2021).
5. Dupuis, C., Lejeune, P., Michez, A. & Fayolle, A. How can remote sensing help monitor tropical moist forest degradation?—a systematic review. *Remote Sens.* **12**, 1087 (2020).
6. Shapiro et al. Forest condition in the Congo Basin for the assessment of ecosystem conservation status. *Ecol. Indic.* **122**, 107268 (2021).
7. Moffette, F., Alix-Garcia, J., Shea, K. & Pickens, A. H. The impact of near-real-time deforestation alerts across the tropics. *Nat. Clim. Chang.* **11**, 1–7 (2021).
8. Tyukavina, A. et al. Congo Basin forest loss dominated by increasing smallholder clearing. *Sci. Adv.* **4**, eaat2993 (2018).
9. Aleman, J. C., Jarzyna, M. A. & Staver, A. C. Forest extent and deforestation in tropical Africa since 1900. *Nat. Ecol. Evol.* **2**, 26–33 (2018).
10. Hansen, M. C. et al. The fate of tropical forest fragments. *Sci Adv* **6**, eaax8574 (2020).
11. Hubau, W. et al. Asynchronous carbon sink saturation in African and Amazonian tropical forests. *Nature* **579**, 80–87 (2020).
12. Csillik, O., Kumar, P., Mascaro, J., O'Shea, T. & Asner, G. P. Monitoring tropical forest carbon stocks and emissions using Planet satellite data. *Sci. Rep.* **9**, 17831 (2019).
13. Harris, N. L. et al. Global maps of twenty-first century forest carbon fluxes. *Nat. Clim. Chang.* https://doi.org/10.1038/s41558-020-00976-6 (2021).
14. Xu, L. et al. Changes in global terrestrial live biomass over the 21st century. *Sci Adv* **7**, eabe9829 (2021).
15. Woodcock, C. E., Loveland, T. R., Herold, M. & Bauer, M. E. Transitioning from change detection to monitoring with remote sensing: a paradigm shift. *Remote Sens. Environ.* **238**, 111558 (2020).
16. Hansen, M. C. et al. High-resolution global maps of 21st-century forest cover change. *Science* **342**, 850–853 (2013).
17. Santoro, M. et al. The global forest above-ground biomass pool for 2010 estimated from high-resolution satellite observations. *Earth Syst. Sci. Data* https://doi.org/10.5194/essd-2020-148 (2020).
18. Reiche, J. et al. Forest disturbance alerts for the Congo Basin using Sentinel-1. *Environ. Res. Lett.* **16**, 024005 (2021).
19. Brancalion, P. H. S. et al. Emerging threats linking tropical deforestation and the COVID-19 pandemic. *Perspect. Ecol. Conserv.* **18**, 243–246 (2020).
20. Wernick, I. K. et al. Quantifying forest change in the European Union. *Nature* **592**, E13–E14 (2021).
21. Araza, A. B. et al. Intra-Annual Identification of Local Deforestation Hotspots in the Philippines Using Earth Observation Products. *Forests* **12**, 1008 (2021).

22. Achard, F. et al. Determination of tropical deforestation rates and related carbon losses from 1990 to 2010. *Glob. Chang. Biol.* **20**, 2540–2554 (2014).
23. FAO. Global Forest Resources Assessment 2020. https://doi.org/10.4060/ca9825en (2020).
24. Sandker, M. et al. The importance of high–quality data for REDD+ monitoring and reporting. *Forests* **12**, 99 (2021).
25. Finer, M. et al. Combating deforestation: from satellite to intervention. *Science* **360**, 1303–1305 (2018).
26. Gorelick, N. et al. Google Earth Engine: planetary-scale geospatial analysis for everyone. *Remote Sens. Environ.* **202**, 18–27 (2017).
27. Turubanova, S., Potapov, P. V., Tyukavina, A. & Hansen, M. C. Ongoing primary forest loss in Brazil, Democratic Republic of the Congo, and Indonesia. *Environ. Res. Lett.* **13**, 074028 (2018).
28. Bunting, P. et al. The Global Mangrove Watch—A New 2010 Global Baseline of Mangrove Extent. *Remote Sens.* **10**, 1669 (2018).
29. Hansen, M. C. et al. Humid tropical forest disturbance alerts using Landsat data. *Environ. Res. Lett.* **11**, 034008 (2016).
30. Hoekman, D. et al. Wide-area near-real-time monitoring of tropical forest degradation and deforestation using sentinel-1. *Remote Sens.* **12**, 3263 (2020).
31. Rosen, P. A. et al. Global persistent SAR sampling with the NASA-ISRO SAR (NISAR) mission. in *2017 IEEE Radar Conference (RadarConf)* 0410–0414 (ieeexplore.ieee.org, 2017).
32. Santoro, M. & Cartus, O. ESA Biomass Climate Change Initiative (Biomass_cci): Global datasets of forest above-ground biomass for the years 2010, 2017 and 2018, v2. (2021).
33. Csillik, O. & Asner, G. P. Near-real time aboveground carbon emissions in Peru. *PLoS ONE* **15**, e0241418 (2020).
34. Dubayah, R. et al. The Global Ecosystem Dynamics Investigation: high-resolution laser ranging of the Earth's forests and topography. *Sci. Remote Sens.* **1**, 100002 (2020).
35. Quegan, S. et al. The European Space Agency BIOMASS mission: measuring forest above-ground biomass from space. *Remote Sens. Environ.* **227**, 44–60 (2019).
36. Olofsson, P. et al. Mitigating the effects of omission errors on area and area change estimates. *Remote Sens. Environ.* **236**, 111492 (2020).
37. Næsset, E. et al. Use of local and global maps of forest canopy height and aboveground biomass to enhance local estimates of biomass in miombo woodlands in Tanzania. *Int. J. Appl. Earth Obs. Geoinf.* **89**, 102109 (2020).
38. Réjou-Méchain, M. et al. Upscaling forest biomass from field to satellite measurements: sources of errors and ways to reduce them. *Surv. Geophys.* **40**, 881–911 (2019).
39. Chave, J. et al. Error propagation and sealing for tropical forest biomass estimates. *Philos. Trans. R. Soc. Lond. B Biol. Sci.* **359**, 409–420 (2004).
40. Rodríguez-Veiga, P. et al. Forest biomass retrieval approaches from earth observation in different biomes. *Int. J. Appl. Earth Obs. Geoinf.* **77**, 53–68 (2019).
41. Araza, A. et al. A comprehensive framework for assessing the accuracy and uncertainty of global above-ground biomass maps. *Remote Sens. Environ.* **272**, 112917 (2022).
42. Dinerstein, E. et al. An ecoregion-based approach to protecting half the terrestrial realm. *Bioscience* **67**, 534–545 (2017).
43. Buchhorn, M. et al. Copernicus global land cover layers—collection 2. *Remote Sens.* **12**, 1044 (2020).
44. Breiman, L. Random forests. *Mach. Learn.* **45**, 5–32 (2001).
45. Greenwell, B. Pdp: an R package for constructing partial dependence plots. *R J.* **9**, 421 (2017).
46. Wager, S., Hastie, T. & Efron, B. Confidence intervals for random forests: the jackknife and the infinitesimal jackknife. *J. Mach. Learn. Res.* **15**, 1625–1651 (2014).
47. IPCC. *IPCC Guidelines for National Greenhouse Gas Inventories*. Vols. 4. Agriculture, Forestry and Other Land Use (2006).
48. Roman-Cuesta, R. M. et al. Hotspots of gross emissions from the land use sector: patterns, uncertainties, and leading emission sources for the period 2000–2005 in the tropics. *Biogeosciences* **13**, 4253–4269 (2016).

Acknowledgements

This study received funding through Norway's Climate and Forest Initiative (NICFI), the US Government's SilvaCarbon program, and was in part supported by the ESA CCI Biomass project and the ESA EO4SD forest management project. This study contains modified Copernicus Sentinel-1 data (2015–2020) and modified ESA Climate Change Initiative BIOMASS data. We thank S. de Bruin for insightful discussions on estimating uncertainty.

Author contributions

O.C., J.R., V.D.S., and M.H. designed the study. O.C. analyzed the data and performed the validation. J.R. provided radar-based alerts and A.A. performed improvements of the biomass product. All authors contributed to the interpretation of the results. J.R., V.D.S., and M.H. supervised the project. O.C. wrote the manuscript with input from all authors.

Competing interests

The authors declare no competing interests.

Additional information

Supplementary information The online version contains supplementary material available at https://doi.org/10.1038/s43247-022-00383-z.

Correspondence and requests for materials should be addressed to Ovidiu Csillik.

Peer review information *Communications Earth & Environment* thanks the anonymous reviewers for their contribution to the peer review of this work. Primary Handling Editors: Gerald Forkuor and Clare Davis.

Reprints and permission information is available at http://www.nature.com/reprints

Publisher's note Springer Nature remains neutral with regard to jurisdictional claims in published maps and institutional affiliations.